

Key role of thermal activation in the electrical switching of antiferromagnetic Mn₂Au

Markus Meinert, Dominik Graulich, and Tristan Matalla-Wagner
*Center for Spinelectronic Materials and Devices, Department of Physics,
 Bielefeld University, D-33501 Bielefeld, Germany**

(Dated: April 4, 2025)

Electrical manipulation of antiferromagnets with specific symmetries offers the prospect of creating novel, antiferromagnetic spintronic devices. Such devices aim to make use of the insensitivity to external magnetic fields and the ultrafast dynamics at the picosecond timescale intrinsic to antiferromagnets. The possibility to electrically switch antiferromagnets was first predicted for Mn₂Au and then experimentally observed in tetragonal CuMnAs. Here, we report on the electrical switching and detection of the magnetization state in epitaxial films of Mn₂Au. The exponential dependences of the switching amplitude on the current density and the temperature are explained by a macroscopic thermal activation model taking into account the effect of the Joule heating in Hall cross devices and we observe that the thermal activation plays a key role in the reorientation process of the magnetization state. Our model analysis shows that the electrically set magnetization is long-term stable at room temperature, paving the way for practical applications in memory devices.

The Néel-order spin-orbit torque (NSOT) was proposed as an efficient mechanism to manipulate the magnetization state of an antiferromagnet.^{1–5} It occurs in layered antiferromagnets with specific symmetries, in particular when the two staggered sublattice magnetic moments \mathbf{m}_A and \mathbf{m}_B are inversion partners. In this case spin polarizations $\mathbf{p}_A = -\mathbf{p}_B$ perpendicular to the current direction occurring due to the inverse spin galvanic effect will give rise to staggered field-like torques $d\mathbf{m}_{A,B}/dt \propto \mathbf{m}_{A,B} \times \mathbf{p}_{A,B}$ on the two sublattices with opposite sign, such that the Néel vector $\mathbf{L} = \mathbf{m}_A - \mathbf{m}_B$ can be aligned perpendicular to the electrical current. Železný et al. predicted the NSOT in Mn₂Au,¹ a tetragonal material of spacegroup $I4/mmm$ with $a = 3.328 \text{ \AA}$ and $c = 8.539 \text{ \AA}$.⁷ Shortly after the prediction, tetragonal CuMnAs,⁸ which belongs to spacegroup $P4/nmm$ was found to have similar magnetic symmetry as Mn₂Au, i.e., that the two magnetic sublattices are connected via inversion. The electrical switching with orthogonal current pulses and readout via the anisotropic magnetoresistance (AMR) and the planar Hall effect (PHE) were demonstrated by Wadley et al. in a star-like microstructure⁶ patterned into an epitaxial CuMnAs film. In their pioneering work, they obtained switching amplitudes on the order of 10 mΩ in both the AHE and PHE and found a strong dependence on the pulse width and the current density used in their switching experiments. Recently, the same group

showed by x-ray magnetic linear dichroism microscopy the direct correlation between antiferromagnetic domain motion and the resistance of a simplified Hall cross device after application of orthogonal current pulses⁹.

EXPERIMENTAL OBSERVATION OF SWITCHING IN MN₂AU

In the present experiment, we investigate the NSOT of epitaxial Mn₂Au films and attempt to explain the observed behaviour with a thermal activation model. To this end, MgO (001) / ZrN 3 nm / Mn₂Au 25 nm / ZrN 2 nm film stacks were grown by dc magnetron co-sputtering and patterned into Hall cross structures as depicted in Figure 1a, similar to the one used by Grzybowski et al.⁹ Current pulse bursts with pulse widths between 100 ns and 10 ms were sent through the crosses and the planar Hall resistance was monitored to observe the switching as sketched in Figure 1b. The bursts are programmed as to keep the transferred charge per burst constant, i.e., at larger current density j_0 , the number of pulses per burst is reduced. As shown in Figure 1b, clear piecewise linear changes of the transverse resistance ΔR_{xy} are seen at current density of $j_0 = 2 \times 10^{11} \text{ A/m}^2$ and pulse width of $\Delta t = 200 \mu\text{s}$, which changes sign when the current pulse direction is switched between two orthogonal directions, very similar to the original experiment by Wadley et al.⁶ A finite-element simulation of the current flow in our experiment shows that the current is very inhomogeneous and hot-spots at the corners of the Hall crosses occur (Figure 1c), which is supported by an optical micrograph of a burnt structure after applying heavy electrical stress (Figure 1d).

MACROSCOPIC MODEL

A systematic investigation of the PHE resistance change (the switching amplitude) per transferred charge as functions of pulse width and current density reveals a very strong dependence of the switching amplitude on either quantity, both suggesting that thermal activation plays a role in the magnetization switching process. To elucidate the role of the thermal activation, we propose a macroscopic model of the switching, based on the key idea that the NSOT provides an effective field that couples to the Néel vector as $\mathbf{L} \cdot \mathbf{B}_{\text{eff}}$, reflecting that the sublattice magnetic moments will feel a Zeeman energy that eventually aligns the Néel vector perpendicular to the current.

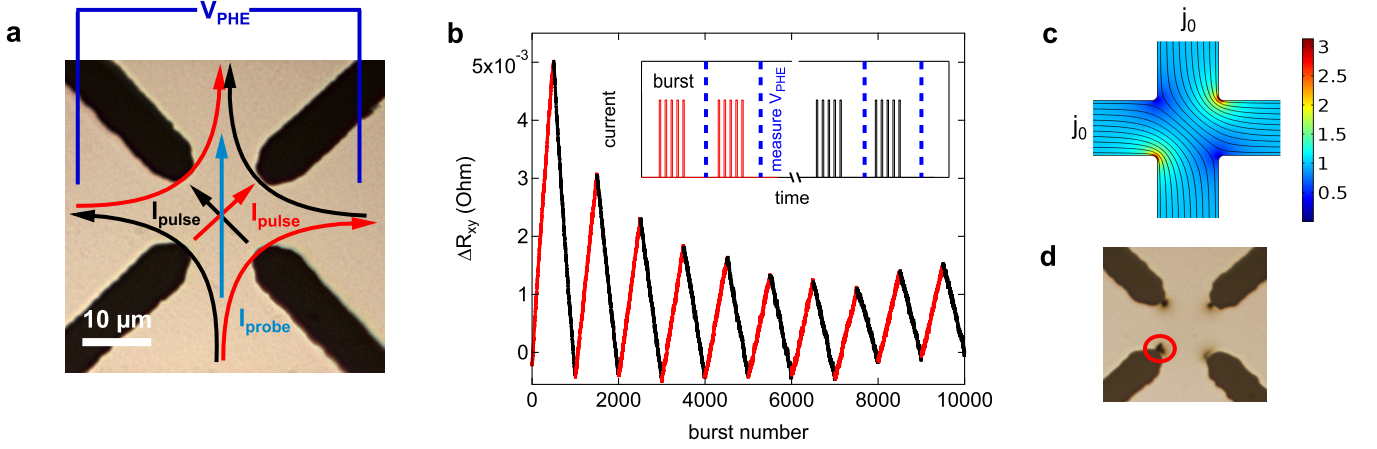


FIG. 1. **Experimental setup and demonstration of magnetization switching.** **a**, Optical micrograph of the Hall cross used for the switching experiment. Current pulses are injected as indicated by red and black curved arrows, resulting in an effective current flow in the center of the Hall cross as indicated by small straight arrows. The Néel vector is thus switched at $\pm 45^\circ$ with respect to both the probe current and the voltage pickup lines, so that the planar Hall effect can be measured at maximum efficiency. **b**, Demonstration of the Néel vector switching at $j_0 = 2 \times 10^{11} \text{ A/m}^2$ and $\Delta t = 200 \mu\text{s}$. Each burst consists of 100 pulses, i.e. 1.92 mC are transferred per burst. The color code reflects the two current directions as specified in **a**. The inset is a graphical representation of the pulse and measurement scheme (not to scale). **c**, finite-element simulation of the current flow. Hot-spots in the cross corners with strongly enhanced local current density are clearly seen. **d**, Optical micrograph of a Hall cross after heavy electrical stress. The film is burnt out in the corners, indicating local current maxima in agreement with the finite-element simulation.

To model the Néel-order spin-orbit torque switching we need to describe the current-induced effective field, the energy barrier for the switching, the Joule heating of the current, and the relation between the Néel vector orientation and the planar Hall effect. The energy barrier for the switching of the Néel vector \mathbf{L} due to the staggered spin-orbit field is written as

$$E_B = K V_g - \mathbf{L} \cdot \mathbf{B}_{\text{eff}} V_g / V_{\text{cell}} \quad (1)$$

with $\mathbf{B}_{\text{eff}} = (\mathbf{j} \times \mathbf{z}) \chi$ being the staggered effective field lying in the plane and perpendicular to the current. K denotes either the biaxial magnetocrystalline anisotropy energy density within the tetragonal (001) plane or an effective pinning energy density for the Néel vector. V_g is the grain volume, \mathbf{j} is the current density in the film plane, \mathbf{z} is the unit vector along the z -axis perpendicular to the film plane, χ is the spin-orbit torque efficiency given as the effective staggered field per unit current density and V_{cell} is the unit cell volume. The first term is the usual magnetocrystalline energy barrier or pinning potential, whereas the second term describes the Zeeman energy of the staggered magnetic moments in the spin-orbit effective field. The Zeeman energy stabilizes the Néel vector such that the sublattice moments will align with the staggered effective field, i.e. perpendicular to the current direction. Because of the very strong exchange interaction in Mn_2Au , each grain is assumed to possess collinear magnetization and has to rotate the Néel vector coherently (the macrospin approximation). The idea to interpret K as a pinning energy density rather than a biaxial anisotropy energy density reflects our observation

that switching is equally possible in both the $[110]$ as well as the $[100]$ directions, in contrast to the biaxial nature of single-crystal Mn_2Au .^{7,10} The imperfect crystal growth of the thin film probably introduces a large number of defects in the film, which are more important for the Néel vector orientation than the intrinsic biaxial anisotropy and allow for arbitrary orientations of the Néel vector in the film plane. The switching rate $1/\tau$ for the switching of the Néel vector of an individual grain into a different orientation is given by the Arrhenius equation

$$\frac{1}{\tau} = f_0 \exp\left(-\frac{E_B}{k_B T}\right), \quad (2)$$

with the attempt rate f_0 , the Boltzmann constant k_B and the absolute temperature T . A similar approach was used to describe the dependence of the antiferromagnetic blocking temperature on the magnetocrystalline anisotropy in exchange bias systems.¹¹ The switching is described by the Poisson distribution, so that the switching probability with an electrical pulse of length Δt can be written as

$$P_{\text{sw}}(\Delta t) = 1 - \exp(-\Delta t/\tau) \quad (3)$$

The influence of the Joule heating of the current density $j = |\mathbf{j}|$ is taken into account by a simplified two-dimensional model as derived by You et al.¹² The Hall cross temperature rise as a function of time is given as

$$\Delta T(t) = \frac{2dj^2}{\sigma \rho_s C_s} \sqrt{\frac{\pi t}{\mu_s}} \operatorname{erf}\left(\frac{w}{4\sqrt{\mu_s t}}\right). \quad (4)$$

Here, d is the film thickness, w is the current line width, σ is the electrical conductivity, ρ_s , C_s , and μ_s are the

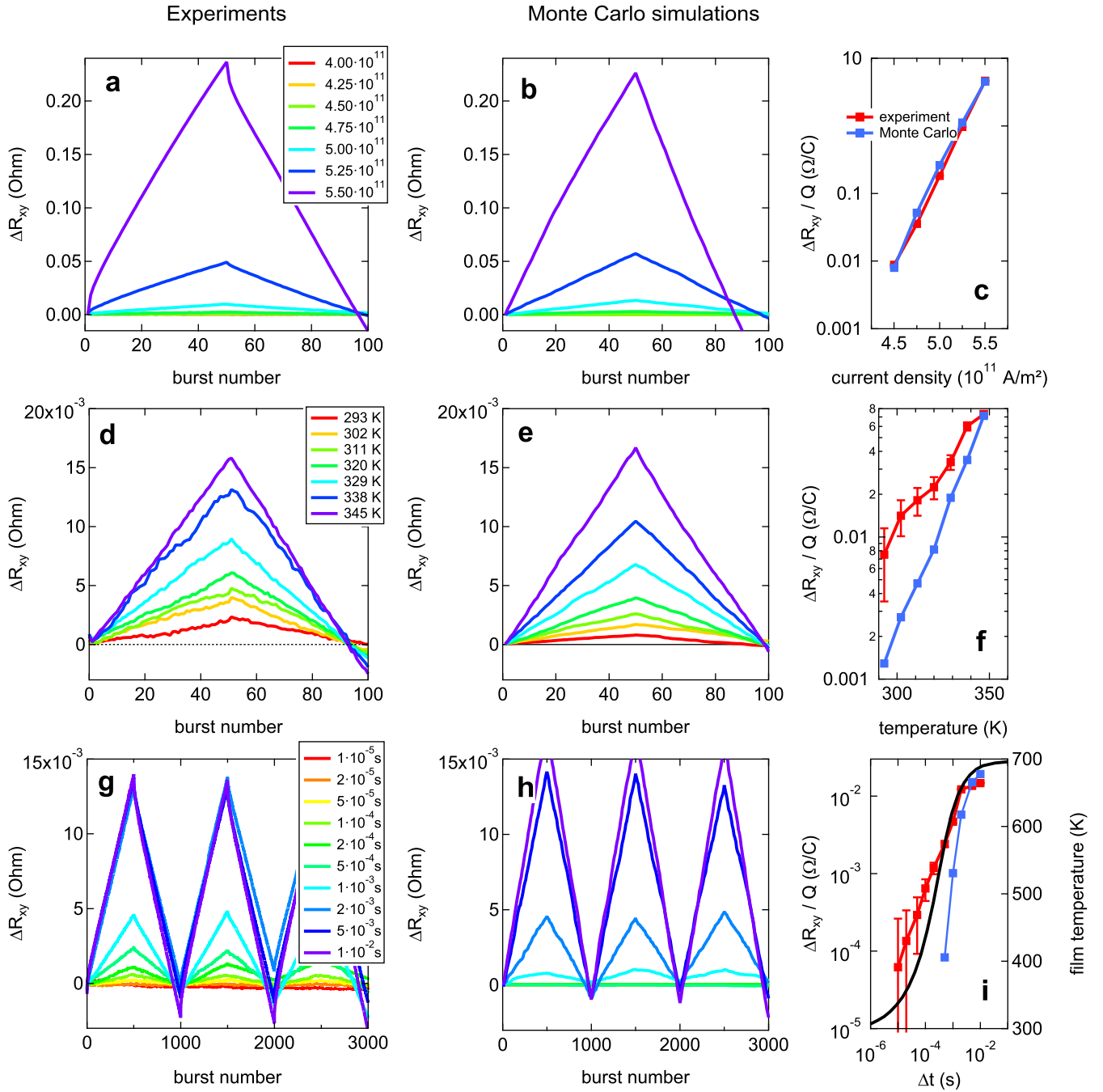


FIG. 2. Measurements of the dependence of the switching amplitude on the current density, base temperature, and pulse width and comparison with the model calculations. **a-c**, switching amplitude as a function of the current density j_0 (given as A/m²). Experiment with $\Delta t = 1 \times 10^{-6}$ s and 1 mC per burst, **a**, Monte Carlo simulations with $D = 15.0$ nm and $K = 17.3 \mu\text{eV}$ per cell, **b**, and extracted switching amplitudes per unit charge (**c**). **d-f**, same as **a-c** for variations of the base temperature with $j_0 = 4.25 \times 10^{11}$ A/m², $\Delta t = 1 \times 10^{-6}$ s, and 5 mC per burst. The Monte Carlo simulations were performed with the same grain size and anisotropy energy as in **b,c**. **g-i**, same as **a-c** for variations of the pulse width with 2 mC per burst and $j_0 = 2 \times 10^{11}$ A/m². Monte Carlo simulations were performed with $D = 18.7$ nm and $K = 17.3 \mu\text{eV}$ per cell, **b**). The black solid line in **i** represents the calculated film temperature according to formula 4

mass density, specific heat, and heat conductivity of the substrate, respectively, and $\mu_s = \kappa_s/(\rho_s C_s)$. The temperature in Eq. 2 is taken as $T = T_0 + \Delta T(\Delta t)$, i.e., the absolute temperature reached at the end of the current pulse duration, where T_0 is the base temperature of the measurement. The orientation of the Néel vector is represented by a polar angle $\varphi \in [0, 2\pi)$. With this angle, the planar Hall effect in our cross geometry is written as $R_{xy} = A \sin(\varphi + \pi/4) \cos(\varphi + \pi/4)$ where the prefactor A is equivalent to the anisotropic magnetoresistance (AMR) amplitude. We note that the model can be easily constrained to the biaxial case by allowing only $\varphi = 0, \pi/2, \pi, 3\pi/2$. Numerical simulations were performed with a Monte Carlo technique as described in the Methods section.

The model does in principle not contain any adjustable parameters and all quantities entering into the equations can be obtained from experiments or *ab initio* calculations. We take $|\mathbf{L}| = 2 \times 4\mu_B$, $V_{\text{cell}} = 4.75 \times 10^{-29} \text{ m}^3$,⁷ and $\chi = 2.0 \times 10^{-11} \text{ mT}/(\text{A}/\text{m}^2)$ ⁶. The film has a resistivity of $73 \times 10^{-8} \Omega\text{m}$ as determined by a four-point measurement and the thermal parameters of the MgO substrate are taken from Ref. 13. The attempt rate f_0 represents the picosecond dynamics of the antiferromagnet,³ so we assume $f_0 = 10^{12} \text{ s}^{-1}$. The core region of the Hall cross has a resistance of about 20Ω and we estimate an AMR amplitude of 5% based on our observations, so that the planar Hall effect amplitude is $A \approx 1 \Omega$. The film thickness is known from x-ray reflectometry. The grain diameter D is taken as the maximum value of the lognormal distribution of grain diameters obtained from an atomic force microscopy measurement (see Supplementary Information) and set to $D = 15 \text{ nm}$. The anisotropy or pinning energy density K remains as the only free parameter of the model, because an independent measurement is not available. Values around $K \approx 18 \mu\text{eV}$ per cell are found to give good agreement with the experimental results. The average current density across the constriction of the Hall cross is used in the calculations, i.e. $j \approx \sqrt{2} \times j_0$.

EXPERIMENTAL AND MODEL RESULTS

In Figure 2a,d,g we show measurements of the switching amplitude for variations of the current density, the base temperature, and the pulse width, in a side-by-side comparison with the corresponding Monte Carlo simulations in Figure 2b,e,h and the extracted amplitudes per unit charge in Figure 2c,f,i. All three datasets are well reproduced by the numerical model calculations with reasonable choices for the anisotropy energy, providing strong evidence for the central role of the thermal activation in the switching process. Specifically, the clear increase of the switching amplitude by increasing the base temperature T_0 of the measurement (Figure 2d) shows that enhanced film temperature due to Joule heating will enhance the switching amplitude. For comparison, we performed calculations of the pulse width and current

density variations without including the effect of Joule heating (not shown). In that case, the dependence on the current density is much less pronounced and the dependence on the pulse width (keeping the transferred charge per burst constant) will vanish completely, in stark contrast with the experiment. Remarkably, the switching amplitude increases exponentially with current density and temperature which is easily seen in the logarithmic plots in Figure 2c,f. The model reproduces these exponential dependencies quite accurately. The discrepancies between the experiments and the model calculations are somewhat larger for the pulse width dependence. Equation 4 predicts a final temperature of nearly 700 K (black solid line in Figure 2i), which is still much smaller than the Néel temperature of Mn_2Au (about 1500 K).⁷ At high temperature, effects from the temperature dependence of the heat conductivity, heat capacity, electrical resistivity, magnetic moments, and anisotropy need to be taken into account, which are omitted in the model. Still, the saturating behaviour at long pulses is reproduced by the calculations.

DISCUSSION

An important consequence of the model is that it allows to estimate the thermal stability of the electrically set magnetization state. Without a current applied, the energy barrier is simply $E_B = KV_g$, which is of the order of 1.6 eV per grain and $K = 58.4 \text{ kJ}/\text{m}^3$ in the present experiment. The thermal stability factor at room temperature $\Delta = E_B/k_B T \approx 64$ is therefore large enough to ensure a stable magnetization state over time scales of more than ten years, thus meeting an important prerequisite for permanent magnetic memories.¹⁴ In Figure 3a we show the extremely strong sensitivity of the switching amplitude on the grain diameter. By increasing the grain diameter by merely 3 nm, one can tune the switching behaviour from saturated to essentially not switchable at a given set of experimental conditions (here $\Delta t = 1 \mu\text{s}$ and 1 mC per burst). The grain size of the films is thus a critical parameter for the NSOT switching behaviour, which equally applies to the film thickness (thinner films are predicted to switch more easily). The initial kinks in the switching seen, e.g., in Figure 2a are therefore explained by the presence of a small number of smaller grains that are easy to saturate, whereas the majority of the grains shows the linear behaviour far off saturation. In all measurements, we find larger switching amplitudes in the first few cycles on a given Hall cross compared to later cycles, where the amplitude remains essentially constant, cf. Fig. 1c. This is explained by the switching in the hot-spots, which see only one current direction in the experiment, so that the Neel vector is reoriented only once and will remain aligned for all further cycles.

Due to the exponential increase of the switching amplitude with increasing current density, saturation of the transverse resistance is expected to be reached by increas-

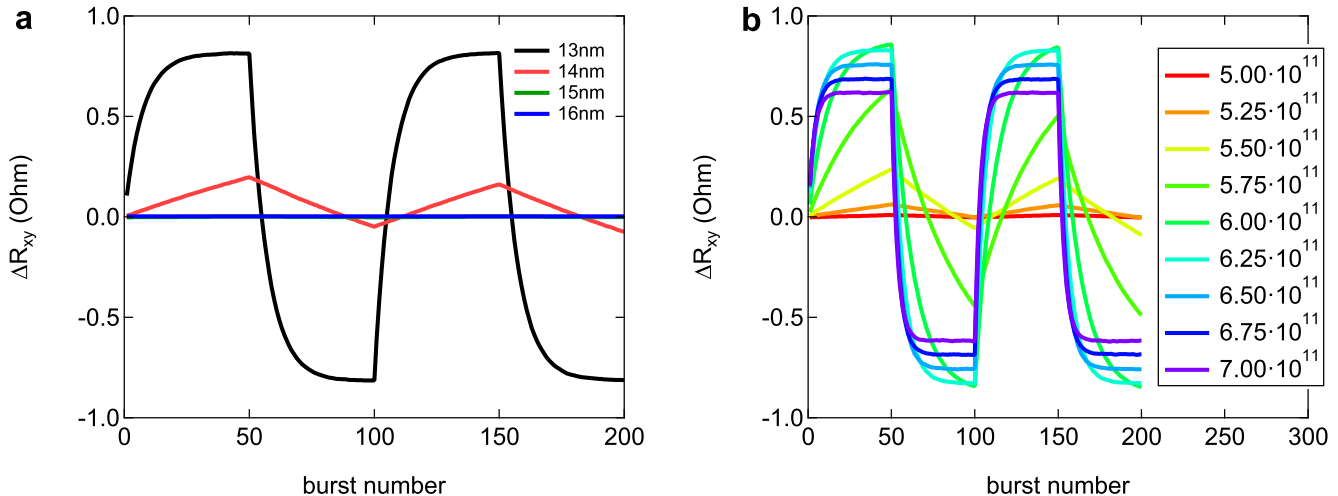


FIG. 3. **Predictions from the Monte Carlo model.** **a**, Calculations with different grain diameters demonstrate a severe dependence of the switching amplitude on the grain size. **b**, Calculations with the same parameters as in Figure 2b but with higher current densities demonstrate saturation and oversaturated behaviour at further increased current (current densities in the legend given as A/m^2).

ing the current density by another ten to twenty percent as shown in Figure 3b. Unfortunately, we were not able to observe the saturated behaviour because no sample withstood a sufficient number of intense current pulses before burning out. A remarkable prediction of our model is that oversaturated switching can be observed at very large current densities due to the exceedingly large thermal fluctuation of the Néel vector, such that the effective NSOT field is not sufficient to fully align the Néel vector anymore. Here we note that the apparently exponential saturation observed by Wadley et al. in CuMnAs ⁶ is now explained by our model calculations as a consequence of the stochastic nature of the switching process and the underlying Poisson probability distribution.

To summarize, we prepared epitaxial Mn_2Au films and demonstrated the electrical switching of the Néel vector. A simple expression for the switching energy barrier is proposed and implemented into a principally parameter-free Monte Carlo model, which shows semi-quantitative agreement with the measurements with realistic model parameters. The Joule heating of the current plays a key role for the switching process, as it provides sufficient thermal activation to reorient the Néel vector with the spin-orbit torque. The switching energy barrier in Mn_2Au is large enough to retain the magnetic state over many years at room temperature, an important condition for the practical application of future antiferromagnetic spintronic devices.

METHODS

Sample fabrication. Thin films of Mn_2Au were grown by dc magnetron co-sputtering of elemental Mn and Au targets

on ZrN buffered MgO substrates, resulting in stacks of the type MgO / ZrN 3 / Mn_2Au 25 / ZrN 2, with film thicknesses in nanometers. The ZrN buffer was deposited by reactive sputtering in an Ar/N mixture at a substrate temperature of 450°C. The Mn_2Au tends to become rough at high deposition temperature, so that the Mn_2Au film used in this study was deposited at 300°C, which results in a compromise between smoothness of the film and crystal quality. The Mn_2Au phase was verified by x-ray diffraction and the film composition was verified by x-ray fluorescence. While Mn_2Au ($a = 3.328 \text{ \AA}$) does not grow well on MgO ($a = 4.21 \text{ \AA}$) due to the large lattice mismatch of 11.5%, it does grow on ZrN. ZrN has a lattice constant ($a = 4.575 \text{ \AA}$) intermediate between those of MgO and Mn_2Au (taking a 45° rotation of the basal plane into account), so that the lattice mismatch is reduced to 2%, rendering it an ideal buffer layer giving rise to the epitaxial relation MgO [100] || ZrN [100] || Mn_2Au [110]. Alternatively, Mn_2Au can be grown on $\text{Al}_2\text{O}_3(1\bar{1}02)$ / Ta substrates,¹⁵ in which case we find a tilt of the c axis of the Mn_2Au with respect to the sample surface of typically 3° and therefore chose to find a growth mode with 4-fold rotational symmetry on MgO. The films were patterned by standard optical photolithography and wire-bonded into IC packages.

Electrical measurements. For the electrical measurements, an arbitrary waveform generator (Agilent 33522A) with a differential broadband amplifier (Tabor Electronics 9260) was used as the voltage source, and a Keithley 2182A Nanovoltmeter was used to measure the planar Hall effect. The switching of the pulse and probe current lines was done with a home-built PhotoMOS switchbox. Temperature-dependent measurements were performed in a closed-cycle He cryostat. A duty cycle of 0.005 and an additional wait time of 1 s before taking the V_{PHE} reading were found to be sufficient to remove cumulative thermal effects within the pulse bursts.

Implementation of the model. The Monte Carlo calculations of the switching model are performed by setting up an ensemble of $N \approx 10^5$ grains with random Néel vec-

tor orientation φ . Optionally, the grain sizes can be taken from any distribution, e.g., a lognormal distribution. Here, only one fixed grain diameter is considered. For each pulse, a random trial configuration is set up and its energy barrier according to Eq. 1 and the switching probability according to Eq. 3 are computed for each grain independently. Random numbers $R \in [0, 1)$ are generated for each grain and the switching into the trial state is accepted if $P_{\text{sw}} > R$. The pulse burst patterns from the experiment are implemented in

the model calculations to accurately reflect the experimental conditions and allow for a one-to-one comparison between the simulated and the experimental data sets. The model allows the magnetization to switch into an arbitrary direction within the sample plane, however, the probability to do so is larger if the sublattice magnetic moments are parallel to staggered effective field. Thus, also thermally activated back-hopping is included in the model and gives rise to the oversaturated behaviour seen in Figure 3c.

-
- * meinert@physik.uni-bielefeld.de
- ¹ Železný, J. et al. Relativistic Néel-Order Fields Induced by Electrical Current in Antiferromagnets. *Phys. Rev. Lett.* 113, 157201 (2014).
 - ² Jungwirth, T., Marti, X., Wadley, P. & Wunderlich, J. Antiferromagnetic spintronics. *Nat. Nanotechnol.* 11, 231241 (2016).
 - ³ Roy, P. E., Otxoa, R. M. & Wunderlich, J. Robust picosecond writing of a layered antiferromagnet by staggered spin-orbit fields. *Phys. Rev. B* 94, 14439 (2016).
 - ⁴ Gomonay, O., Jungwirth, T. & Sinova, J. High Antiferromagnetic Domain Wall Velocity Induced by Néel Spin-Orbit Torques. *Phys. Rev. Lett.* 117, 17202 (2016).
 - ⁵ Gomonay, O., Jungwirth, T. & Sinova, J. Concepts of antiferromagnetic spintronics. *Phys. Status Solidi RRL* 11, 1700022 (2017).
 - ⁶ Wadley, P. et al. Electrical switching of an antiferromagnet. *Science* 351, 587590 (2016).
 - ⁷ Barthem, V. M. T. S., Colin, C. V., Mayaffre, H., Julien, M.-H. & Givord, D. Revealing the properties of Mn2Au for antiferromagnetic spintronics. *Nat. Commun.* 4, 2892 (2013).
 - ⁸ Wadley, P. et al. Tetragonal phase of epitaxial room-temperature antiferromagnet CuMnAs. *Nat. Commun.* 4, 2322 (2013).
 - ⁹ Grzybowski, M. J. et al. Imaging Current-Induced Switching of Antiferromagnetic Domains in CuMnAs. *Phys. Rev. Lett.* 118, 57701 (2017).
 - ¹⁰ Barthem, V. M. T. S., Colin, C. V., Haettel, R., Dufeu, D. & Givord, D. Easy moment direction and antiferromagnetic domain wall motion in Mn2Au. *J. Magn. Magn. Mater.* 406, 289292 (2016).
 - ¹¹ OGrady, K., Fernandez-Outon, L. E. & Vallejo-Fernandez, G. A new paradigm for exchange bias in polycrystalline thin films. *J. Magn. Magn. Mater.* 322, 883899 (2010).
 - ¹² You, C.-Y., Sung, I. M. & Joe, B.-K. Analytic expression for the temperature of the current-heated nanowire for the current-induced domain wall motion. *Appl. Phys. Lett.* 89, 222513 (2006).

- ¹³ Stackhouse, S., Stixrude, L. & Karki, B. B. Thermal Conductivity of Periclase (MgO) from First Principles. *Phys. Rev. Lett.* 104, 208501 (2010).
- ¹⁴ Khvalkovskiy, A. V. V et al. Basic principles of STT-MRAM cell operation in memory arrays. *J. Phys. D. Appl. Phys.* 46, 74001 (2013).
- ¹⁵ Jourdan, M. et al. Epitaxial Mn2Au thin films for antiferromagnetic spintronics. *J. Phys. D. Appl. Phys.* 48, 385001 (2015).

ACKNOWLEDGEMENTS

The authors thank D. Kappe for providing the finite-element simulation of the Hall cross device. They further thank G. Reiss for making available the laboratory equipment.

AUTHOR CONTRIBUTIONS

M.M. guided the experiment, developed the model and implemented it. D.G. and T.M.-W. prepared the samples, carried out the electrical measurements and contributed to building the setup. M.M. wrote the manuscript. All authors discussed the results and commented on the manuscript.

ADDITIONAL INFORMATION

Supplementary information is available in the online version of the paper. Correspondence and requests for materials should be addressed to M.M.

COMPETING FINANCIAL INTERESTS

The authors declare no competing financial interests.

Key role of thermal activation in the electrical switching of antiferromagnetic Mn_2Au - Supplementary Information -

Markus Meinert, Dominik Graulich, and Tristan Matalla-Wagner
*Center for Spinelectronic Materials and Devices, Department of Physics,
Bielefeld University, D-33501 Bielefeld, Germany**

(Dated: April 4, 2025)

In Figure 1 we show x-ray diffraction measurements of Mn_2Au films grown on MgO substrates with a ZrN buffer layer at different substrate temperatures. Pure phase Mn_2Au is found for all temperatures between 250°C and 450°C. However, the preferential orientation of the grains is improved as the temperature is increased, eventually giving pure (001)-oriented films at 450°C. For the electrical switching study, a deposition temperature of 300°C was chosen, because the resistivity is rather large ($73 \mu\Omega\text{cm}$) and shows only weak temperature dependence, so that

our constant-voltage source can be treated as a constant-current source and the current density can be simply obtained from Ohm's law with the room-temperature resistance value.

In Figure 2 we provide an atomic force microscopy (AFM) image of the film deposited at 300°C. In the right panel of Figure 2, the manually evaluated grain size analysis is shown together with a lognormal fit to the histogram. For simplicity, we take the maximum probability grain diameter, $D_{\text{max}} \approx 15 \text{ nm}$ as the grain diameter entering into the thermal activation model.

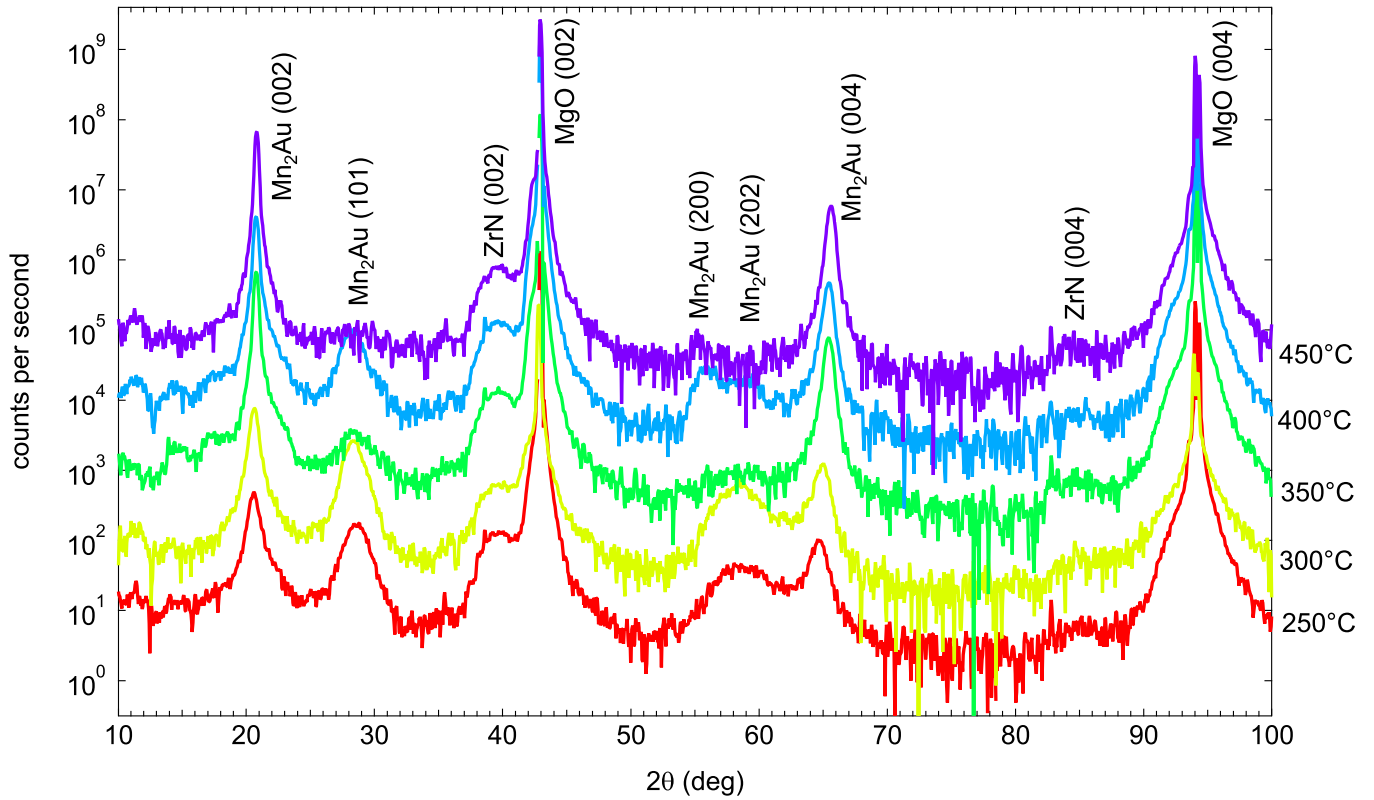


FIG. 1. X-ray diffraction measurements on MgO / ZrN 3 / Mn₂Au 25 / ZrN 2 stacks with the Mn₂Au layer deposited at temperatures between 250°C and 450°C.

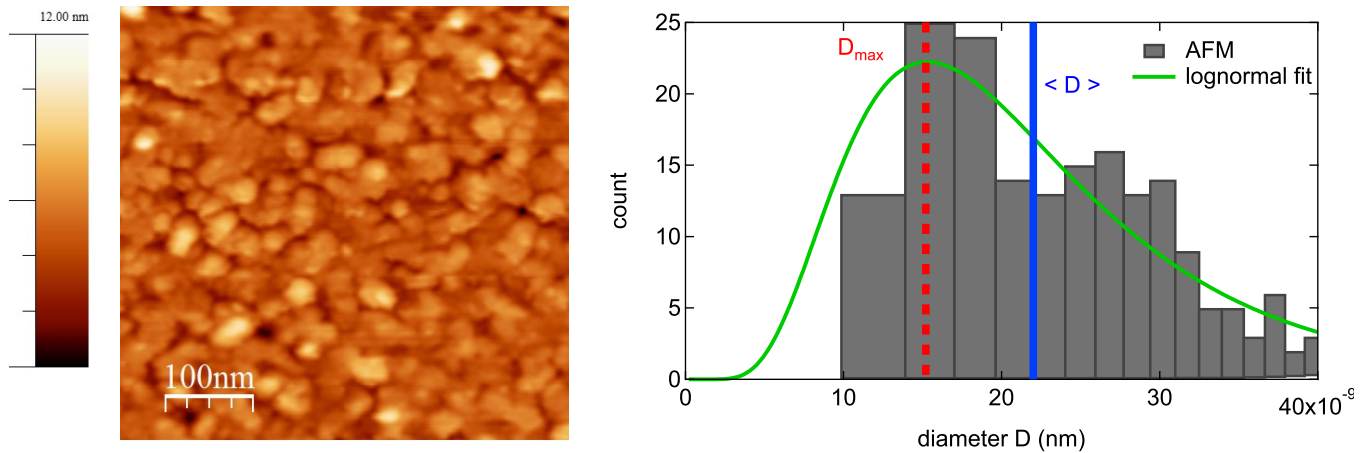


FIG. 2. Left: Atomic force microscopy image of the MgO / ZrN 3 / Mn₂Au 25 / ZrN 2 stack with Mn₂Au deposited at 300°C used in the electrical switching study discussed in the main text. Right: Histogram of the manual grain diameter analysis of about 200 grains from the AFM picture with a lognormal fit and average and maximum probability diameters indicated by $\langle D \rangle$ and D_{\max} , respectively. Smaller diameters than 10 nm are not reliably obtained from the picture.